

Unmasking the Nodal Quasiparticle Dynamics in Cuprate Superconductors Using Low-Energy Photoemission

T. Yamasaki,¹ K. Yamazaki,¹ A. Ino,¹ M. Arita,² H. Namatame,² M. Taniguchi,^{1,2}
A. Fujimori,³ Z.-X. Shen,⁴ M. Ishikado,⁵ and S. Uchida⁵

¹*Graduate School of Science, Hiroshima University, Higashi-Hiroshima 739-8526, Japan*

²*Hiroshima Synchrotron Radiation Center (HSRC),*

Hiroshima University, Higashi-Hiroshima 739-8526, Japan

³*Department of Complexity Science and Engineering, University of Tokyo, Kashiwa 277-8561, Japan*

⁴*Department of Physics, Applied Physics and Stanford Synchrotron Radiation Laboratory,
Stanford University, Stanford, CA 94305, USA and*

⁵*Department of Physics, University of Tokyo, Tokyo 113-0033, Japan*

(Dated: December 2, 2024)

Nodal quasiparticles of $\text{Bi}_2\text{Sr}_2\text{CaCu}_2\text{O}_{8+\delta}$ have been studied by angle-resolved photoemission spectroscopy with an unprecedented momentum-resolution. Low-energy tunable photons have enabled us to resolve a small nodal bilayer splitting, unmasking intrinsic single-particle scattering rate. The nodal scattering rate is abruptly suppressed upon the superconducting transition, and shows a linear energy-dependence, indicating the nontrivial effect of elastic scatterings on the quasiparticles. The difference between the bilayer-resolved scattering rates hints the nature of impurities involved.

PACS numbers: 74.72.Hs, 74.25.Jb, 79.60.-i

Thermodynamics properties of a superconductor both in the zero-field and vortex-mixed states are governed by excitations of low-energy quasiparticles. They are particularly important for a d -wave superconductor, where the gap has a node and therefore the excitations start from the zero-energy. Nevertheless, probing the nodal scattering rate is often difficult due to the masking by the superconductivity itself. To date, the quasiparticle scattering rate over extended temperature range has been deduced from ac transport properties: microwave and optics experiments on high- T_c cuprates indicate a dramatic suppression of the scattering rate below T_c [1, 2, 3, 4]. However, with increasing the quasiparticle energy, the selective study of the nodal direction is difficult for the transport experiments. In addition, the interpretation of the optical data is not unique, and the validity of the extended Drude model has long been debated.

Angle-resolved photoemission spectroscopy (ARPES) can provide direct information on the single-quasiparticle excitations underlying intricately-integrated transport properties. No specific model is required to extract the quasiparticle scattering rate and dispersion from the spectral peak width and position, respectively. For this reason, serious ARPES experiments have been attempted so far [5, 6, 7, 8, 9, 10], but the results were controversial. For example, an ARPES report has proposed that the marginal-Fermi-liquid behavior persists into the superconducting state [6]. No discontinuity has been identified at T_c in the temperature dependence of the scattering rate [6, 7], in contrast with the transport experiments [1, 2, 3, 4, 11]. The monotonous energy dependence of the quasiparticle scattering rate [6, 10] is inconsistent with the observation of the abrupt change in the quasiparticle velocity at ~ 70 meV [7, 8, 9]. The residual quasiparticle-

momentum width, $\Delta k \simeq 0.02 \text{ \AA}^{-1}$, has been unexpectedly wider than the instrumental resolution [6, 7, 10].

In this paper, we show a new ARPES result obtained using low-energy excitation photons ($h\nu = 7.57$ eV). The controversies are clearly resolved by sharp ARPES images ($\Delta k = 0.0065 \text{ \AA}^{-1}$). Based on the detailed temperature- and energy-dependence of the scattering rate, we argue that the low-energy quasiparticles are seriously affected by the elastic scattering process. Furthermore, bilayer-resolved scattering rates imply a spatial dependence of the scattering potential.

The low-energy tunable photons have advantages in precise ARPES experiments. First, in-plane quasiparticle momenta k_{\parallel} are magnified into large emission angles. The higher momentum resolution is realized by a given instrumental angular resolution. Second, the effect of possible surface imperfection and contamination is minimized, because of the longer photoelectron escape depth. According to the universal curve [12], the escape depth for $h\nu = 7.57$ eV is one order of magnitude longer than that, $< 10 \text{ \AA}$, for the conventional energy, $h\nu \sim 20$ eV. Although the escape depth for the cuprates remains to be checked, it is reasonable to assume that it becomes much longer for $h\nu = 7.57$ eV [13]. Third, the selectivity is improved, filtered by the well-defined final state of a long escape depth. For instance, the surface-normal momentum k_{\perp} is better resolved [14]. However, since low-energy final states have a structure unlike free electrons, tuning the photon energy to the final state is critically important in order to enable the photoemission. Here, we optimized the photon energy so that both the bonding and antibonding bands are clearly observed.

The ARPES experiments were performed at a helical undulator beamline, BL-9 at Hiroshima Synchrotron

Radiation Center, using a SCIENTA SES2002 analyzer. The total energy resolution was set at 4 meV, and the angular resolution is confirmed to be better than 0.5° , which corresponds to a momentum of 0.007 \AA^{-1} at $h\nu = 7.57 \text{ eV}$. Samples are nearly optimally doped $\text{Bi}_2\text{Sr}_2\text{CaCu}_2\text{O}_{8+\delta}$ ($T_c = 86 \text{ K}$), which were cleaved *in situ* under an ultrahigh vacuum, $< 1 \times 10^{-10} \text{ Torr}$.

Results at a low temperature of $T = 9 \text{ K}$ are shown in Figs. 1 and 2, which demonstrate the performance of the low-energy ARPES. First, Fig. 1 clearly shows that the nature of quasiparticle excitations dramatically changes at an energy of $|\omega| \sim 70 \text{ meV}$, as compared with the “kink” observed so far [7, 8, 9, 10]. The quasiparticle peak is strikingly sharpened on crossing $|\omega| \sim 70 \text{ meV}$ towards the Fermi level, in good correlation with the abrupt deceleration of the quasiparticle group velocity $v_k = d\omega_k/dk$. Second, as shown in Fig. 2, the peak becomes so sharp near $\omega = 0$ that the previously unresolved small splitting of 0.0075 \AA^{-1} is distinctly observed. The quasiparticle momentum width of $\Delta k = 0.0065 \text{ \AA}^{-1}$ at $\omega = 0$ is much sharper than before [6, 7, 10], and reveals that the nodal quasiparticles travel for long, $\geq 150 \text{ \AA}$, without scattering in the superconducting state.

Peaks of the doublet in Fig. 2(c) are identified as the bonding and antibonding bands of two proximate CuO_2 layers. Such bilayer splitting has recently been resolved around the antinode [15, 16] and considered to vanish

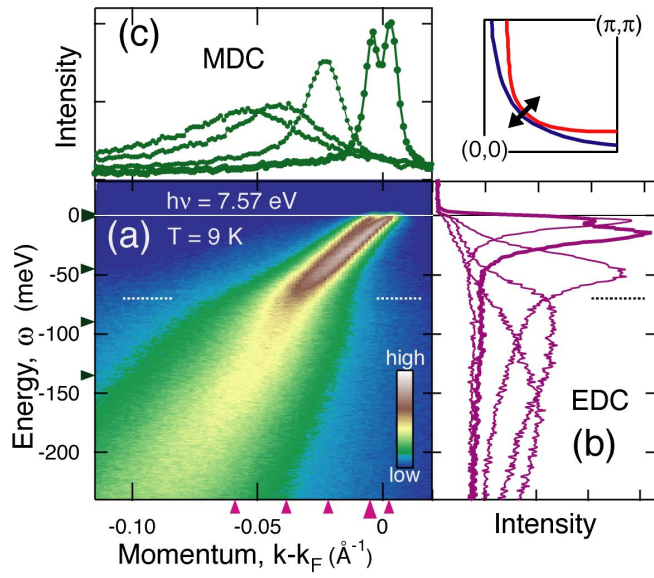


FIG. 1: Overview of low-energy ARPES result at $h\nu = 7.57 \text{ eV}$, taken in the nodal direction of superconducting $\text{Bi}_2\text{Sr}_2\text{CaCu}_2\text{O}_{8+\delta}$ at $T = 9 \text{ K}$. (a) Spectral-intensity map in the energy-momentum space. White dotted lines indicate the characteristic energy, $|\omega| \sim 70 \text{ meV}$. (b) Energy distribution curves (EDCs) at the momenta denoted by purple triangles. (c) Momentum distribution curves (MDCs) at the energies denoted by green triangles. The intensity of the MDC at $\omega = 0$ is multiplied by 2.

at the node previously, because the primary intrabilayer hoppings via $\text{Cu } 4s$ orbitals, t_{ss}^\perp and t_{sp}^\perp , are forbidden by the absence of the hybridization between $d_{x^2-y^2}$ and s orbitals [17]. We have carefully confirmed that the splitting width, $k_b - k_a = 0.0075 \pm 0.001 \text{ \AA}^{-1}$, is reproduced for several samples. Multiplying $k_b - k_a$ by the experimental Fermi velocity $v_F = 1.9 \text{ eV\AA}$ gives the nodal splitting energy, $\omega_a - \omega_b = 14 \pm 1 \text{ meV}$, much smaller than 23 meV reported by Kordyuk *et al* [18]. Compared to the antinodal splitting of $\sim 88 \text{ meV}$ [15, 16], the nodal splitting of 14 meV indicates the presence of the non-negligible p - p transfer, t_{pp}^\perp [18]. The widths of the bilayer-split peaks are resolved as shown in Fig. 2(d) by fitting each momentum distribution curve (MDC) with two independent Lorentzians. The result indicates that the scattering rate has a linear energy-dependence near $\omega = 0$.

The temperature dependence of the spectral function is shown in Fig. 3. While the spectral feature is substantially unchanged in the superconducting state ($T = 9$ and 50 K), the quasiparticle peak near $\omega = 0$ is remarkably broadened in the normal state ($T = 95$ and 200 K). We have extended the MDC-fitting analysis to high temperatures and high energies by regarding splitting parameters as constants, i.e. relative peak position $k_b - k_a = 0.0075 \text{ \AA}^{-1}$, width $\Delta k_a/\Delta k_b = 1$, and intensity $I_a/I_b = 0.78$,

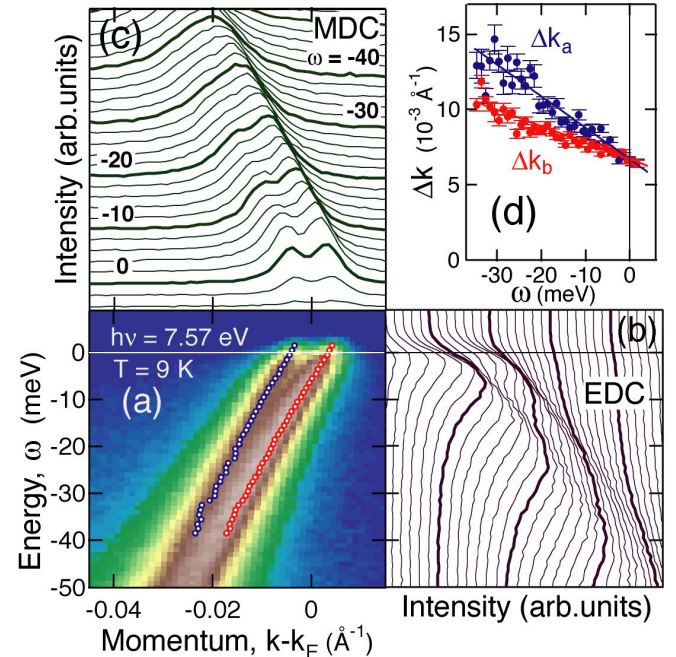


FIG. 2: Enlarged view of Fig. 1 around the Fermi-surface crossings. (a) Spectral-intensity map. Red and blue circles denote the peak positions of the MDCs. (b) EDCs at each 0.0012 \AA^{-1} . (c) MDCs at each 2 meV . (d) Bilayer-resolved scattering rates, determined from the momentum widths (FWHM), Δk_b (red) and Δk_a (blue), of the bonding and antibonding peaks, respectively. Thin solid lines show the linear increasing rates, ~ 0.11 and $\sim 0.21 \text{ \AA}^{-1}\text{eV}^{-1}$, of Δk_b and Δk_a , respectively.

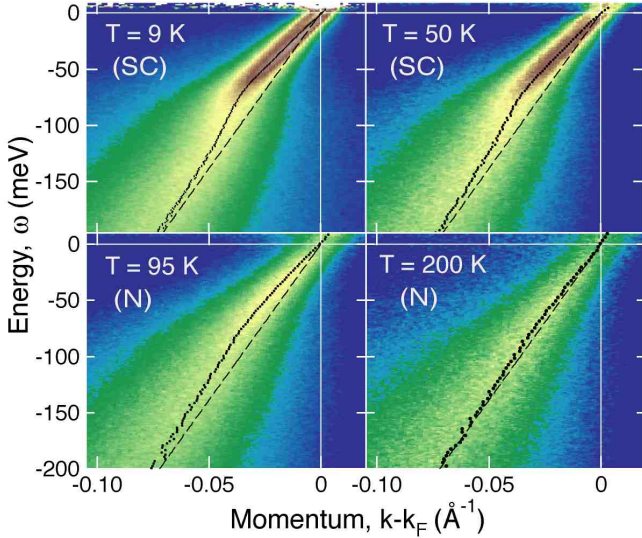


FIG. 3: Single-particle spectral function in the superconducting ($T = 9$ and 50 K) and normal ($T = 95$ and 200 K) states, obtained by dividing the ARPES intensity by the Fermi-Dirac distribution function. Dotted and thin dashed lines denote the weighted center of the bonding and antibonding peaks in the MDCs, and the hypothetical unrenormalized dispersion $\epsilon_k^0' = v_0'(k - k_F)$ for $v_0' = 2.8$ eVÅ, respectively.

and obtained the average momentum width and dispersion of the bonding and antibonding quasiparticles.

Figures 4(a) and (b) show the quasiparticle renormalization energy and scattering rate, i.e. the real and imaginary parts of the self-energy $\Sigma(\omega)$, respectively. They are causally dependent on each other in reality, but we have derived them from independent spectral features. The real part, $\text{Re}\Sigma'(\omega)$, has been deduced from the dispersion deviation from a straight line. The imaginary part, $\text{Im}\Sigma(\omega)$, is directly given by the momentum width, namely the inverse scattering length, at the scaling factor of a constant unrenormalized velocity [19]. Figures 4(c) and (d) show that the width-derived $\text{Im}\Sigma(\omega)$ is consistent with the Kramers-Krönig transformation $\text{Im}\Sigma'_{\text{KK}}(\omega)$ of the dispersion-derived $\text{Re}\Sigma'(\omega)$ [20]. The step features of $\text{Im}\Sigma(\omega)$ and $\text{Im}\Sigma'_{\text{KK}}(\omega)$ agree excellently in the position $50 \leq |\omega| \leq 90$ meV and in the height ~ 35 meV. On taking the difference, the bump at $|\omega| \sim 90$ meV is cancelled out at all the temperatures. The monotonous increase in $\text{Im}\Sigma(\omega) - \text{Im}\Sigma'_{\text{KK}}(\omega)$ with $|\omega|$ may be ascribed to the electron-electron scattering, because $\text{Re}\Sigma'(\omega)$ is exclusive of the ω -linear term without cutoff such as the electron-electron scatterings of the Fermi liquid, $\text{Im}\Sigma_{\text{el-el}}^{\text{FL}} \propto \omega^2$. On the other hand, collective bosonic modes such as phonons usually have a low cutoff energy, and thus contribute both to $\text{Re}\Sigma'(\omega)$ and $\text{Im}\Sigma(\omega)$. In contrast to the marginal-Fermi-liquid scenario [6], the present $\text{Im}\Sigma(\omega)$ and $\text{Re}\Sigma'(\omega)$ consistently indicate that the scattering rate abruptly increases from $|\omega| = 50$ to 90 meV due to the coupling with the bosonic modes.

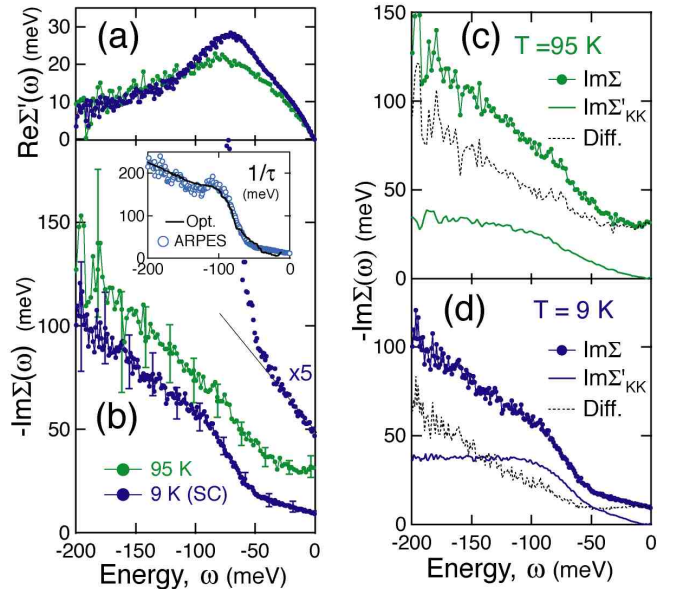


FIG. 4: Self-energy $\Sigma(\omega)$ in the nodal direction, obtained by the MDC-fitting analysis regarding the splitting parameters as constants. (a) Real part of self-energy, determined from the quasiparticle dispersion by $\text{Re}\Sigma'(\omega_k) = \omega_k - \epsilon_k^0'$. (b) Imaginary part of self-energy, determined from the quasiparticle momentum width Δk (FWHM) by $\text{Im}\Sigma(\omega) = -\frac{1}{2}v_0\Delta k$, where the scaling factor is $v_0 = 2.8$ eVÅ [19]. Fivefold magnified view shows the ω -linear fit (black line) of $\text{Im}\Sigma(\omega)$ at $T = 9$ K. Inset shows the inverse lifetimes, deduced from ARPES by $1/\tau(\omega) = v_k\Delta k$ (open circles) and from optical conductivity (line) [4]. (c)(d) Comparison between the width-derived $\text{Im}\Sigma(\omega)$ (filled circles) and the Kramers-Krönig transformation $\text{Im}\Sigma'_{\text{KK}}(\omega)$ (solid lines) of the dispersion-derived $\text{Re}\Sigma'(\omega)$ for $T = 95$ and 9 K. The bump at $|\omega| \sim 90$ meV is cancelled out in the difference, $\text{Im}\Sigma(\omega) - \text{Im}\Sigma'_{\text{KK}}(\omega)$ (black dotted lines).

The inverse scattering time, $1/\tau(\omega)$, is also deduced from the momentum width multiplied by the quasiparticle group velocity, $1/\tau(\omega) = \Delta E = v_k\Delta k$. The inset of Fig. 4(b) compares the nodal single-particle scattering rate obtained by ARPES with the transport scattering rate derived from the optical conductivity [4]. The overall similarity in quantity indicates that the extrinsic broadening of the ARPES spectral peak is minimized by using the low-energy excitation photons.

Figure 5 shows the temperature-dependence of the MDC and scattering rate at $\omega = 0$. We have found that the momentum width of the nodal quasiparticle is abruptly suppressed by ~ 0.01 Å⁻¹ (60-70 % drop) upon the superconducting transition ($T_c = 86$ K). This observation reconciles the ARPES results with the transport studies [1, 2, 3, 4, 11]. Note that the residual scattering rate in the superconducting state is lower than the normal-state scattering rate linearly extrapolated to $T \rightarrow 0$. In conventional two-dimensional Fermi liquid, the inelastic part of the zero-energy scattering rate decreases for $T \rightarrow 0$ as the higher-order power than T

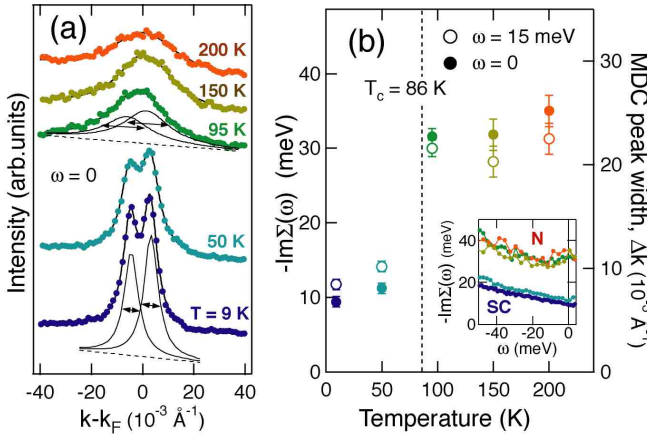


FIG. 5: (a) Temperature dependence of the MDC at $\omega = 0$. The spectral peaks are dramatically sharpened in the superconducting state. (b) Temperature dependence of the scattering rate, $\text{Im}\Sigma(\omega) = -\frac{1}{2}v_0\Delta k$, determined from the momentum width Δk (FWHM) at $\omega = 0$ (filled circles) and 15 meV (open circles). Inset shows the scattering rate as a function of energy for the superconducting (SC) and normal (N) states.

linear, $\text{Im}\Sigma_{\text{inel}}^{\text{FL}}(0) \propto T^n (n > 1)$. Even in marginal Fermi liquid, it decreases linearly, $\text{Im}\Sigma_{\text{inel}}^{\text{MFL}}(0) \propto T$ [6, 21]. Thus, Fig. 5(b) suggests that the reduction of the scattering rate at T_c occurs not only for the inelastic part but also for the elastic part. This implies that the elastic impurity scattering is no more constant unlike in normal metal, but has a serious energy-dependent effect on the low-energy quasiparticles [22, 23]. In the normal state, a zero-energy electron is elastically scattered into the other segment of the Fermi surface. The opening of the d -wave superconducting gap would close these scattering channels except for those into the other nodal points. Consequently, the nodal quasiparticles are hardly scattered by the impurities in the superconducting state, even though the superconducting gap is closed there.

In the nodal quasiparticle scattering rate for $|\omega| \lesssim 40$ meV, the ω -linear term appears to predominate over the ω^3 term [24, 25] in the superconducting state, as shown in Figs. 2(d) and 4(b). Since the low-energy electronic density of states is proportional to $|\omega|$ due to the d -wave gap, the elastic scattering rate may have an ω -linear term, while the inelastic scattering rate only have the higher order term negligible at low energies [23]. The sources of the elastic scatterings are implied by that the ω -linear term is smaller for the bonding-band scattering rate than for the antibonding one, as shown in Fig. 2(d). If impurities are distant from the quasiparticles, the scattering angles are small, and the scattering destination is restricted to around the node, as proposed recently [21, 22, 23]. Then, with increasing $|\omega|$, few scattering channels are opened [23]. Because the bonding band has more probability amplitude inside the CuO_2 bilayer, the impurities are likely outside the CuO_2 bilayer, e.g. antisite defects

or excess oxygens in the BiO and SrO layers [22, 23, 26].

In conclusion, the low-energy ARPES has unmasked the intrinsic quasiparticle behaviors unique to the node, implying the necessity to reexamine all the quasiparticles. The bilayer-resolved quasiparticle properties provide an internal reference for the nature of the scattering.

We thank P. J. Hirschfeld, D. J. Scalapino, A. Kimura and K. Shimada for enlightening discussion. This study was performed under the Cooperation Research Program of HiSOR, Hiroshima Synchrotron Radiation Center, Hiroshima University (Proposal No. 04-A-19), and partially supported by Grant-in-Aids for Young Scientists and for Scientific Research in Priority Area “Invention of Anomalous Quantum Materials” from the Ministry of Education, Culture, Sports, Science and Technology of Japan.

- [1] D. A. Bonn *et al.*, Phys. Rev. B **47**, 11314 (1993).
- [2] D. A. Bonn *et al.*, Phys. Rev. Lett. **68**, 2390 (1992).
- [3] A. Hosseini *et al.*, Phys. Rev. B **60**, 1349 (1999).
- [4] A. V. Puchkov, D. N. Basov, and T. Timusk, J. Phys. **8**, 10049 (1996).
- [5] A. Damascelli, Z. Hussain, and Z.-X. Shen, Rev. Mod. Phys. **75**, 473 (2003).
- [6] T. Valla *et al.*, Science **285**, 2110 (2001); T. Valla *et al.*, Phys. Rev. Lett. **85**, 828 (2000); Z. M. Yusof *et al.*, Phys. Rev. Lett. **88**, 167006 (2002).
- [7] A. Kaminski *et al.*, Phys. Rev. Lett. **84**, 1788 (2000); A. Kaminski *et al.*, *ibid.* **86**, 1070 (2001).
- [8] A. Lanzara *et al.*, Nature **412**, 510 (2001).
- [9] P. D. Johnson *et al.*, Phys. Rev. Lett. **87**, 177007 (2001).
- [10] A. A. Kordyuk *et al.*, Phys. Rev. Lett. **92**, 257006 (2004).
- [11] J. Takeya *et al.*, Phys. Rev. Lett. **88**, 077001 (2002).
- [12] M. P. Seah and W. A. Dench, Surf. and Interface Anal. **1**, 2 (1979).
- [13] M. R. Norman, M. Randeria, H. Ding and J. C. Campuzano, Phys. Rev. B **59**, 11191 (1999).
- [14] N. V. Smith *et al.*, Phys. Rev. B **47**, 15476 (1993).
- [15] D. L. Feng *et al.*, Phys. Rev. Lett. **86**, 5550 (2002).
- [16] Y. D. Chuang *et al.*, Phys. Rev. Lett. **87**, 117002 (2001).
- [17] O. K. Andersen *et al.*, J. Phys. Chem. Solids **56**, 1573 (1995).
- [18] A. A. Kordyuk *et al.*, Phys. Rev. B **70**, 214525 (2004).
- [19] On the presumption that the momentum dependence of $\Sigma(\omega, k)$ is much smaller than the energy dependence, $\text{Im}\Sigma(\omega) = -\frac{1}{2}v_0\Delta k$, where Δk is the momentum width and v_0 is the unrenormalized velocity .
- [20] S. Verga *et al.*, Phys. Rev. B **67**, 054503 (2003).
- [21] E. Abrahams and C. M. Varma, PNAS. **97**, 5714 (2000).
- [22] D. J. Scalapino, T. S. Nunner, and P. J. Hirschfeld, cond-mat/0409204.
- [23] L. Zhu *et al.*, Phys. Rev. B **70**, 214503 (2004); T. Dahm, P. J. Hirschfeld, D. J. Scalapino, and L. Zhu, Phys. Rev. B **72**, 214512 (2005).
- [24] S. M. Quinlan, D. J. Scalapino, and N. Bulut, Phys. Rev. B **49**, 1470 (1994).
- [25] M. L. Titov, A. G. Yashenkin, and D. N. Aristov, Phys. Rev. B **52**, 10626 (1995).
- [26] H. Eisaki *et al.*, Phys. Rev. B **69**, 064512 (2004).